Study of $MnXO_4 \cdot nH_2O$ (X = P, As) Phases and Synthesis and Structure of the Simple, Novel Salt $MnAsO_4$

Miguel A. G. Aranda,*,† J. Paul Attfield,‡ and Sebastian Bruque†

Departamento de Química Inorgánica, Facultad de Ciencias, Universidad de Málaga, 29071 Málaga, Spain, and Department of Chemistry, University of Cambridge, Lensfield Road, Cambridge CB2 1EW, U.K.

Received August 21, 1992

$Mn^{III}XO_4 \cdot nH_2O$ (X = P, As; n = 1.0–1.5) phases have been characterized through electron microscopy, density measurements, thermal analysis, and X-ray powder diffraction. Samples with $n > 1$ behave as intergrowths of stoichiometric, crystalline $MnXO_4 \cdot H_2O$ and amorphous $MnXO_4 \cdot mH_2O$ with $m \sim 4$. A detailed study of the thermal behavior of these systems has revealed that the presence of the amorphous phase strongly affects the dehydration and reduction temperatures. The phosphate and arsenate always decompose through different pathways, as the phosphate undergoes reduction of Mn^{3+} to Mn^{2+} before water loss commences, whereas the arsenate shows a reversible dehydration before being irreversibly reduced. This has enabled the simple new salt $MnAsO_4$ to be prepared by careful decomposition of $MnAsO_4 \cdot nH_2O$, and the crystal structure (monoclinic, space group $P2_1/n$, a = 6.679(3) Å, b = 8.940(3) Å, c = 4.791(2) Å, β = 93.76(4)°) has been determined from laboratory X-ray powder diffraction data using the Rietveld method (R_{WP} = 7.4%, R_P = 5.5%, and R_F = 2.7%). This arrangement is a unique example of a monoclinically-distorted $CuSO_4$ type structure. Chains of edge-sharing MnO_6 octahedra containing two different Mn^{3+} sites that display cooperative [4 + 2] and [2 + 2 + 2] Jahn–Teller distortions are linked through distorted AsO_4 groups.

Introduction

Metal phosphates and arsenates are currently of interest for their chemical and physical properties, and resulting applications as catalysts, nonlinear optical materials, ion exchangers, and ionic and electronic conductors.[1] For example, vanadium pyrophosphate, $(VO)_2P_2O_7$, is used to catalyze the oxidation of butane and butene to maleic anhydride;[2] $KTiOPO_4$ is a well-known nonlinear optical material;[3] $M^{IV}(HPO_4)H_2O$ (M = Zr, Sn, Ti, Hf) compounds comprise an important family of highly stable ionic exchangers;[4] $M^IM^{IV}_2(PO_4)_3$ (M^I = Li, Na, K, Rb, Cs; M^{IV} = Zr, Hf) compounds are fast ion conductors of the NASICON family.[5] On the other hand, phosphates and arsenates of the first-row transition metals exhibit a wide range of interesting magnetic properties. For example, the superexchange interactions between octahedrally coordinated spin-only cations have been studied in a number of MXO_4 (X = P, As) compounds.[6–8] As part of this effort, we are currently undertaking a detailed synthetic, structural, spectroscopic, and reactivity study of manganese(III) phosphates and arsenates. These materials provide synthetic challenges, as Mn^{3+} is prone to oxidation or reduction when heated or in aqueous solution.

Several complex manganese(III) phosphates such as the mixed-valence mineral Bermanite, $Mn_3(PO_4)_2(OH)_2 \cdot 4H_2O$,[9] manganese(III) metaphosphate, $Mn(PO_3)_3$,[10] manganese(III) hydrogen pyrophosphate, $MnHP_2O_7$,[11] manganese(III) dihydrogen triphosphate dihydrate, $MnH_2P_3O_{10} \cdot 2H_2O$[12] and the layered materials $KMn_2O(PO_4)(HPO_4)$[13] and $NH_4Mn_2O(PO_4)(HPO_4) \cdot H_2O$[14] are known. No analogous arsenates have been reported, although hydrates $MnXO_4 \cdot nH_2O$ are known for X = P and As.

A polycrystalline manganese(III) phosphate hydrate $MnPO_4 \cdot nH_2O$ was first synthesized by Christensen[15] from manganese(III) acetate and phosphoric acid and also through the oxidation of manganese(II) nitrate by nitric acid in the presence of phosphoric acid. The degree of hydration of this phase has been controversial. Goloschapov and Martinenko[16] proposed that n = 1.5, and this was corroborated by several authors.[12,17–19] Narita and Okabe found 1.13 water molecules per formula unit,[20,21] but Cudennec et al.[22] established that n could vary from 1 to 1.7 without appreciably modifying the powder X-ray diffraction pattern. We have recently synthesized analogous arsenates $MnAsO_4 \cdot nH_2O$, and we observe a similar variation of n = 1–1.5 without changes in the powder X-ray pattern.[23]

The crystal structures of $Mn^{III}XO_4 \cdot nH_2O$ (X = P,[24] As[23]) have been determined from powder X-ray diffraction data and have recently been refined precisely with 4 K neutron diffraction profiles

* To whom correspondence should be addressed. Current address: Department of Chemistry, University of Cambridge.
† Universidad de Málaga.
‡ University of Cambridge.

(1) *Eur. J. Solid State Inorg. Chem.* **1991**, *28*. Special Issue.
(2) Hodnett, B. K.; Permanne, P.; Delmon, B. *Appl. Catal.* **1983**, *6*, 231.
(3) Bierlein, J. D.; Vanherzeele, J. *J. Opt. Soc. Am. B.* **1989**, *6*, 622.
(4) Clearfield, A. In *Inorganic Ion Exchange Materials*; CRC Press: Boca Raton, FL, 1982.
(5) Clearfield, A. *Chem. Rev.* **1988**, *88*, 125.
(6) Battle, P. D.; Gibb, T. C.; Hu, G.; Munro, D. C.; Attfield, J. P. *J. Solid State Chem.* **1986**, *65*, 343.
(7) Attfield, J. P.; Cheetham, A. K.; Johnson, D. C.; Torardi, C. C. *Inorg. Chem.* **1987**, *26*, 3379.
(8) Attfield, J. P.; Battle, P. D.; Cheetham, A. K.; Johnson, D. C. *Inorg. Chem.* **1989**, *28*, 1207.
(9) Kampk, A. R.; Moore, P. B. *Am. Mineral.* **1976**, *61*, 1241.
(10) Bagieu-Beucher, M. *Acta Crystallogr.* **1978**, *B34*, 1443.
(11) Durif, A.; Averbuch-Pouchot, M. T. *Acta Crystallogr.* **1982**, *B38*, 2883.
(12) Selevich, A. F.; Lyutsko, V. D. *Zh. Neorg. Khim.* **1984**, *29*, 629; *Russ. J. Inorg. Chem. (Engl. Transl.)* **1984**, *29*, 364.
(13) Lightfoot, P.; Cheetham, A. K.; Sleight, A. W. *J. Solid State Chem.* **1988**, *73*, 325.
(14) Lightfoot, P.; Cheetham, A. K. *J. Solid State Chem.* **1988**, *78*, 17.
(15) Christensen, O. T. *J. Prakt. Chem.* **1883**, *28*, 1.
(16) Goloschapov, M. V.; Martinenko, B. V. *Zh. Neorg. Khim.* **1976**, *21*, 1357; *Russ. J. Inorg. Chem. (Engl. Transl.)* **1976**, *21*, 742.
(17) Teterevkov, A. I.; Chubarov, A. V. *Zh. Neorg. Khim.* **1982**, *27*, 943; *Russ. J. Inorg. Chem. (Engl. Transl.)* **1982**, *27*, 529.
(18) Boyle, F. W.; Lindsay, W. L. *Soil Sci. Soc. Am. J.* **1985**, *49*, 758.
(19) Boyle, F. W.; Lindsay, W. L. *Soil Sci. Soc. Am. J.* **1986**, *50*, 588.
(20) Narita, E.; Okabe, T. *Ind. Eng. Chem. Prod. Res. Dev.* **1982**, *21*, 662.
(21) Narita, E.; Okabe, T. *Bull. Chem. Soc. Jpn.* **1983**, *56*, 2841.
(22) Cudennec, Y.; Riou, A.; Gerault, Y. *C. R. Acad. Sci., Ser. 2* **1986**, *302*, 1149.
(23) Aranda, M. A. G.; Bruque, S.; Attfield, J. P. *Inorg. Chem.* **1991**, *30*, 2043.
(24) Lightfoot, P.; Cheetham, A. K.; Sleight, A. W. *Inorg. Chem.* **1987**, *26*, 3544.

0020-1669/93/1332-1925$04.00/0

of deuterated samples showing that $n = 1$ in both cases.[25] The two compounds are isomorphous with the stoichiometric metal(II) sulfates $MSO_4 \cdot H_2O$ (M = Mg, Mn, Fe, Co, Ni, Zn),[26,27] and no evidence for additional water within the structure was found nor is there sufficient space to accommodate it. The $MnXO_4 \cdot H_2O$ structure consists of axially distorted MnO_6 octahedra linked by the oxygen atom of the water molecule at a common vertex to form zigzag Mn–O–Mn chains. These chains are interconnected by XO_4 tetrahedra to form a three-dimensional network with small channels running parallel to the c axis, into which the hydrogen atoms of the water molecules project.

We have recently investigated the magnetic properties of the $MnXO_4 \cdot H_2O$ (X = P, As) compounds[25] and their lithium-exchange reactions to give $LiMnXO_4(OH)$ derivatives.[28,29] In order to understand the chemistry of these $MnXO_4 \cdot nH_2O$ materials, and variations in their reported thermal behavior and densities,[30] we have performed this systematic investigation of the water content of the $MnPO_4 \cdot nH_2O$ and $MnAsO_4 \cdot nH_2O$ systems. We have also investigated the use of these materials as precursors for possible, previously unknown $MnXO_4$ compounds. Such MXO_4 salts are of fundamental interest for the packing of cations and tetrahedral oxo-anions and for their magnetic properties.

Experimental Section

$MnXO_4 \cdot nH_2O$ (X = P, As) materials were synthesized under atmospheric conditions and autogenous hydrothermal pressures up to 10 bar. The atmospheric pressure samples were prepared by slowly adding 85% H_3PO_4 or 75% H_3AsO_4 to an aqueous suspension of manganese(II) carbonate hydrate. After a release of CO_2, nitric acid was added and the reaction mixtures were boiled to oxidize Mn(II) to Mn(III), which resulted in the evolution of NO_2 and the formation of dark green precipitates. Hydrothermal syntheses were performed by heating mixtures of Mn_2O_3, 85% H_3PO_4 or 75% H_3AsO_4, and H_2O in approximate Mn:X:H_2O molar ratios of 1:3:30 at 200 °C for 2 weeks in Teflon-lined autoclaves. The products from both routes were filtered out, washed with water and acetone, and dried at 70 °C.

Samples of $MnAsO_4$ were obtained by heating $MnAsO_4 \cdot nH_2O$ (n = 1–1.5) at low temperatures to minimize the reduction to $Mn_2As_2O_7$, but this could not be completely avoided. The best ratio of $MnAsO_4$ to $Mn_2As_2O_7$ was obtained by heating $MnAsO_4 \cdot 1.5H_2O$ at 325 (±5) °C until none of the precursor hydrate remained (~50 h). The dehydration reaction was found to be reversible; after 2 weeks of standing in air diffraction peaks of $MnAsO_4 \cdot H_2O$ were seen in the $MnAsO_4$ samples.

Water contents were measured from the weight change after heating at 800 °C for several hours, allowing for the loss of oxygen due to the reduction of manganese(III) to manganese(II). Combined thermogravimetric (TGA) and differential (DTA) thermal analyses were carried out in air on a Rigaku Thermoflex apparatus at a heating rate of 10 K/min with calcined Al_2O_3 as the reference. Pycnometric density measurements were performed with reagent grade acetone of density 0.7899 Mg m^{-3} as the filling solution.[19,31] Transmission electron micrographs and electron diffraction patterns were obtained on a JEOL 2000FX electron microscope.

X-ray diffraction patterns were recorded on a Siemens D501 automated diffractometer using graphite-monochromated Cu Kα radiation. The diffraction profile used to refine the structure of $MnAsO_4$ was collected in the 20 range 18–120° counting for 16 s/0.03° step. These data were transferred to a VAX 8530 computer for Rietveld analysis[32] by the multiphase GSAS program[33] using a pseudo-Voigt peak shape function corrected for asymmetry at low angles and a refined background function.

To estimate the proportions of amorphous $MnXO_4 \cdot mH_2O$ and crystalline $MnXO_4 \cdot H_2O$ phases in the atmospheric pressure samples, a quantitative powder X-ray diffraction analysis was carried out by an internal standard method.[34] Calibration graphs for X = P and As were constructed using four different mixtures of crystalline $MnXO_4 \cdot H_2O$ (X = P, As) and KCl as the internal standard with a weight percent of $MnXO_4 \cdot H_2O$ between 85 and 95%. X-ray diffraction scans were recorded between 27.5 and 31° (2θ), with a step size of 0.02° and a counting time of 7 s/point. The areas of the two nonoverlapping peaks (KCl, (002) at d = 3.141 Å; $MnXO_4 \cdot H_2O$, (202) at d = 2.954, 2.994 Å for X = P, As) were extracted using the program DRX.[35] Atmospheric pressure $MnXO_4 \cdot nH_2O$ samples were then ground with KCl (90% of $MnXO_4 \cdot nH_2O$ and 10% of KCl), and from the ratio of the diffraction peak areas and the calibration graph, the amount of crystalline $MnXO_4 \cdot H_2O$ was determined. Hence, knowing the total amount of sample and the amount of crystalline phase, the amount of amorphous $MnXO_4 \cdot mH_2O$ was determined.

Results and Discussion

$MnXO_4 \cdot nH_2O$ Phases. Preparations at ambient and hydrothermal pressures always resulted in samples containing $MnXO_4 \cdot H_2O$ as the only crystalline phase in the X-ray diffraction pattern. However, TGA showed that the hydrothermal products were stoichiometric with $n = 1.0$, whereas nonstoichiometric materials with n = 1.1–1.5 resulted from the atmospheric pressure syntheses. The morphology and microcrystallinity of $MnAsO_4 \cdot nH_2O$ products with $n = 1.0$ and 1.5 were investigated by electron microscopy. The hydrothermal $n = 1.0$ phase was found to contain well-formed microcrystallites that gave sharp diffraction spots (Figure 1a), whereas particles of the $n = 1.5$ material appeared poorly crystalline and gave near-polycrystalline electron diffraction patterns (Figure 1b).

Results of the density study are given in Table I. For the stoichiometric, hydrothermally synthesized samples, the agreement between the measured density values and those calculated from the crystallographic data is very good. For the samples with $n > 1$, the observed values are lower than those for the crystalline samples, indicating the presence of a second less dense phase. This fact would explain the disagreement between the previously reported density value for $MnPO_4 \cdot nH_2O$ and the calculated X-ray one.[30]

The TGA–DTA curves for $MnPO_4 \cdot nH_2O$ and $MnAsO_4 \cdot nH_2O$ are shown in Figures 2 and 3, respectively. These systems retain water strongly, as the weight losses for all the samples never start until at least 280 °C in air at the heating rate of 10 °C/min. The thermal behavior of the $MnAsO_4 \cdot nH_2O$ samples is different from that of the analogous phosphates, as has been reported previously,[23] since the reduction of Mn(III) to Mn(II) takes place after the water loss whereas the phosphate is reduced before being dehydrated. Hence, it should be possible to obtain $MnAsO_4$ but not $MnPO_4$ by careful decomposition of the hydrate, as is described below.

The temperatures of the endotherms are given in Table I and are assigned from the associated weight losses. These results demonstrate that the temperatures of the decomposition processes of the $MnXO_4 \cdot nH_2O$ phases depend strongly upon n, suggesting that crystalline $n = 1.0$ and amorphous $n > 1$ phases are intergrown within the same particles of these materials. In particular, the loss of the water molecule from the crystalline phases is displaced to lower temperatures with increasing amounts of amorphous material, from 495 °C for $MnPO_4 \cdot H_2O$ to 475 °C for $MnPO_4 \cdot 1.2H_2O$ and from 465 °C for $MnAsO_4 \cdot H_2O$ to 325 °C for

(25) Aranda, M. A. G.; Attfield, J. P.; Bruque, S.; Palacio, F. *J. Mat. Chem.* **1992**, *2*, 501.
(26) Coing-Boyant, J.; Bassi, G. *C. R. Acad. Sci.* **1963**, *256*, 1482.
(27) Bregeault, J. M.; Herpin, P.; Manoli, J. M.; Pannetier, G. *Bull. Soc. Chim. Fr.* **1970**, 4243.
(28) Aranda, M. A. G.; Attfield, J. P.; Bruque, S. *J. Chem. Soc., Chem. Commun.* **1991**, 604.
(29) Aranda, M. A. G.; Attfield, J. P.; Bruque, S. *Angew. Chem. Int. Ed. Engl.* **1992**, *31*, 1090.
(30) The calculated crystallographic density for the sample, $MnPO_4 \cdot H_2O$, is 3.173 Mg m^{-3}, in disagreement with the reported datum 2.57 Mg m^{-3}, for the sample formulated as $MnPO_4 \cdot 1.5H_2O$,[19] although with identical powder X-ray diffraction pattern.
(31) *Chemical Rubber Co. Handbook of chemistry and physics*, 56th ed., Chemical Rubber Co. Press: Cleveland, OH, 1976.
(32) Rietveld, H. M. *J. Appl. Crystallogr.* **1969**, *2*, 65.
(33) Larson, A. C.; Von Dreele, R. B. Los Alamos National Laboratory Report No. LA-UR-86-748, 1987.
(34) Whiston, C. *X-Ray Methods*; F. E. Prichard: London, 1987; pp 121–131.
(35) Vila, E.; Ruiz-Amil, A.; Martín, J. L. DRX, Program for the analysis of X-ray powder diffraction patterns, CSIC, Madrid, 1989.

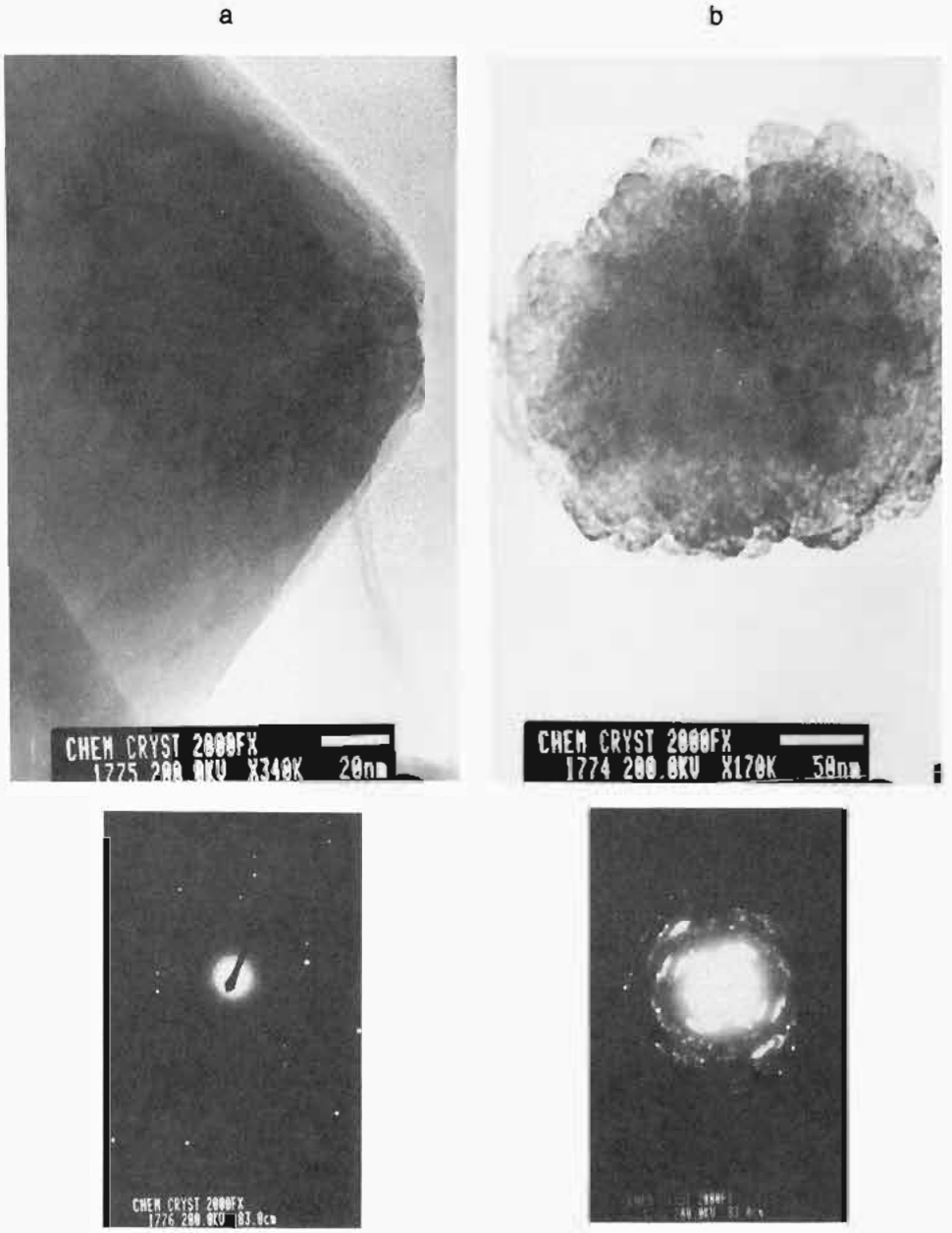

Figure 1. Transmission electron micrographs and electron diffraction patterns of (a) $MnAsO_4 \cdot H_2O$ and (b) $MnAsO_4 \cdot 1.5H_2O$.

Table I. Density and Thermal Analysis Results for the $MnXO_4 \cdot nH_2O$ (X = P, As) Samples

samples	density (Mg m^{-3})			endotherm temp (°C)		
	ρ_{theor}	ρ_{exp}	n	H_2O amorphous phase	H_2O crystalline phase	O_2
$MnPO_4 \cdot H_2O$	3.173	3.16(5)	0.97(4)		470	495
$MnPO_4 \cdot 1.2H_2O$		2.84(6)	1.20(4)	300	380	475
$MnAsO_4 \cdot H_2O$	3.697	3.63(5)	1.02(4)		465	575, 680
$MnAsO_4 \cdot 1.2H_2O$			1.23(4)	340	425	580, 775
$MnAsO_4 \cdot 1.5H_2O$		3.26(6)	1.52(4)	325[a]	325[a]	630, 750

[a] These endotherms are overlapped.

$MnAsO_4 \cdot 1.5H_2O$. This correlation may be a kinetic phenomenon, reflecting smaller domains of the crystalline phase within the intergrown particles with higher n. As n increases for the $MnAsO_4 \cdot nH_2O$ materials, the separation between the endotherms corresponding to water loss and reduction of Mn(III) to Mn(II) becomes greater. This observation implies that the greatest ratio of $MnAsO_4$ to $Mn_2As_2O_7$ should be observed by decomposing materials with the largest n, which we have found to true. The loss of the O_2 from $MnAsO_4$ takes place in two steps for all the $MnAsO_4 \cdot nH_2O$ samples, suggesting that an intermediate mixed Mn^{II}, Mn^{III} phase is formed, although we have not seen evidence for this in the X-ray diffraction patterns.

The above electron microscopy, density, and TGA–DTA results strong suggest that $MnXO_4 \cdot nH_2O$ (X = P, As) compositions with $n > 1$ are intergrowths of crystalline $MnXO_4 \cdot H_2O$ and amorphous material of mean composition $MnXO_4 \cdot mH_2O$, although the results shown above are also consistent with a mixture of crystalline and amorphous phases, with smaller particle sizes at higher average water contents. In order to estimate the proportions of these two phases, and the value of m, an analytical powder X-ray diffraction study was carried out, as described in the Experimental Section. This showed a sample of $MnPO_4 \cdot 1.12H_2O$ to contain 95% of crystalline $MnPO_4 \cdot H_2O$ and a 5% of amorphous $MnPO_4 \cdot mH_2O$, and $MnAsO_4 \cdot 1.52H_2O$ con-

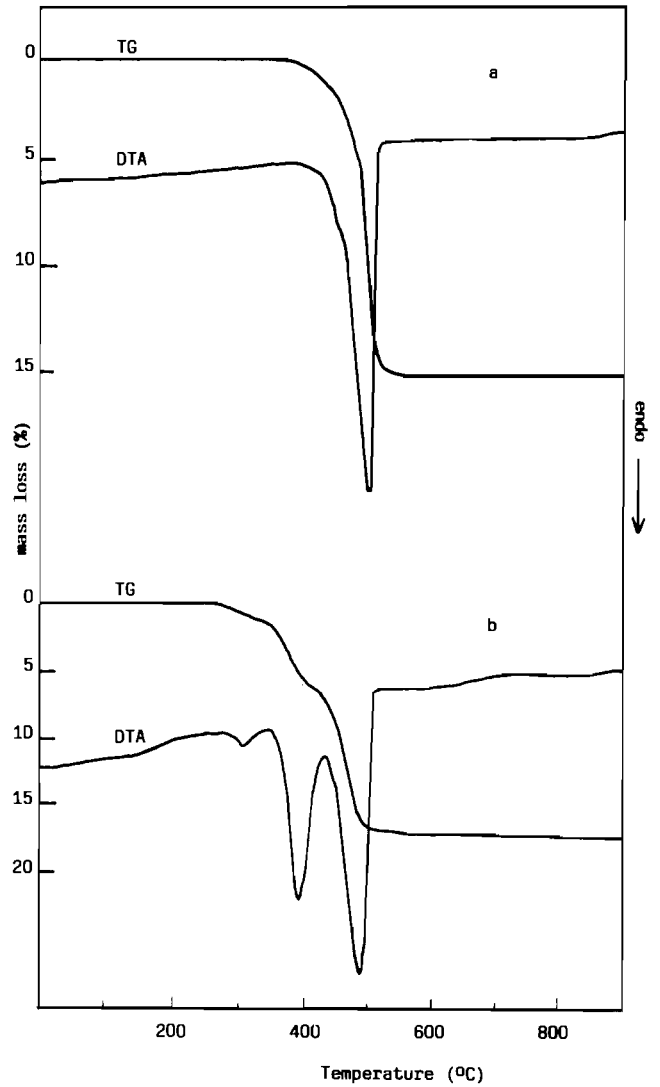

Figure 2. Thermal analyses (TGA and DTA) for (a) $MnPO_4 \cdot H_2O$ and (b) $MnPO_4 \cdot 1.2H_2O$.

tained 84% of crystalline $MnAsO_4 \cdot H_2O$ and 16% of $MnAsO_4 \cdot mH_2O$. From these results we derive the mean values of $m = 4(1)$ for the phosphate and arsenate. Hence the amorphous phases in both systems are of approximate average composition $MnXO_4 \cdot 4H_2O$.

Taken together, these results reveal a two-step mechanism for the formation of the crystalline $MnXO_4 \cdot H_2O$. Initial reaction between aqueous Mn^{3+} and XO_4^{3-} results in the rapid precipitation of amorphous $MnXO_4 \cdot mH_2O$ with $m \sim 4$. This value suggests that the reaction occurs through the facile substitution of two water molecules by XO_4^{3-} in the Jahn–Teller distorted $3d^4$ $Mn(H_2O)_6^{3+}$ cation. The kinetic $MnXO_4 \cdot mH_2O$ phase loses water to give crystalline $MnXO_4 \cdot H_2O$ through nucleation of $MnXO_4 \cdot H_2O$ microcrystallites within the particles of the amorphous phase. This reaction proceeds to completion under hydrothermal pressure, but at ambient conditions the reported products $MnXO_4 \cdot nH_2O$ with $n \sim 1$–1.7[12,15–23] are intergrowths of the amorphous precursor and the crystalline monohydrate.

$MnAsO_4$. After the exclusion of the peaks from $Mn_2As_2O_7$, the powder pattern of $MnAsO_4$ was autoindexed by the program Treor[36] from the accurately measured positions of 16 nonoverlapping reflections, using KCl as an internal standard. A monoclinic cell of dimensions $a = 6.679(3)$ Å, $b = 8.940(3)$ Å, $c = 4.791(2)$ Å, and $\beta = 93.76(4)°$ was obtained with figures of merit $M_{16} = 23$[37] and $F_{16} = 21$ (0.013, 59).[38] This cell is similar

(36) Werner, P. E. *Z. Krystallogr.* **1969**, *120*, 375.

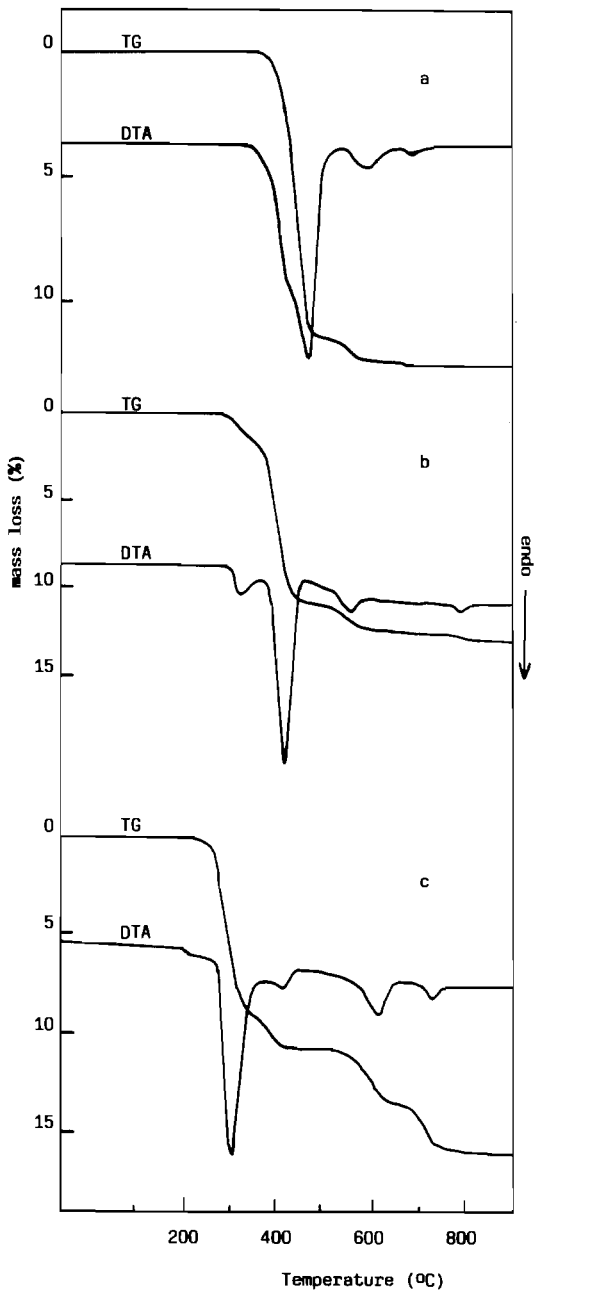

Figure 3. Thermal analyses (TGA and DTA) for (a) $MnAsO_4 \cdot H_2O$, (b) $MnAsO_4 \cdot 1.2H_2O$, and (c) $MnAsO_4 \cdot 1.5H_2O$.

to that of orthorhombic $CuSO_4$[39,40] (space group *Pmnb*, $a = 6.709$ Å, $b = 8.409$ Å, $c = 4.833$ Å), so we attempted to fit the X-ray profile of the $Mn_2As_2O_7/MnAsO_4$ mixture using our previously determined structure of $Mn_2As_2O_7$[23] and taking the coordinates of $CuSO_4$[40] as a starting model for $MnAsO_4$ with the space group symmetry reduced from orthorhombic *Pmnb* to monoclinic $P2_1/n$. For $Mn_2As_2O_7$, only the scale factor and peak shape parameters were varied, but a full refinement of these parameters plus cell constants, atomic coordinates, and isotropic temperature factors was performed for $MnAsO_4$, giving $R_{WP} = 7.4\%$, $R_P = 5.5\%$, and $R_F(MnAsO_4) = 2.7\%$. Results of the refinement are given in Tables II and III, and the final observed, calculated, and difference profiles are given in Figure 4. The use of a multiphase refinement program enables a good refinement of $MnAsO_4$ to be obtained as this is the major component of the mixture. The molar composition of the mixture determined from the scale factors of

(37) Wolff, P. M. d. *J. Appl. Crystallogr.* **1968**, *1*, 108.
(38) Smith, G. S.; Snyder, R. L. *J. Appl. Crystallogr.* **1979**, *12*, 60.
(39) Kokkoros, P. A.; Rentzeperis, P. J. *Acta Crystallogr.* **1958**, *11*, 361.
(40) Wildner, M.; Giester, G. *Miner. Petrology* **1988**, *39*, 201.

Table II. Structural Parameters for $MnAsO_4$ in Space Group $P2_1/n$ (No. 14) from the Refinement of the $MnAsO_4/Mn_2As_2O_7$ Mixture

Refinement Data

no. of allowed reflcns: 426 for $MnAsO_4$ and 226 for $Mn_2As_2O_7$
no. of points in refinement: 3400 no. of variables: 36
scale factors per formula units: $S(MnAsO_4) = 159.8(6)$; $S(Mn_2As_2O_7) = 44.9(3)$

Cell Data

$a = 6.6833(2)$ Å $b = 8.9303(2)$ Å $c = 4.7914(1)$ Å $\beta = 93.813(2)°$
$V = 285.34(2)$ Å^3 $Z = 4$

R Factors (%)[a]

$R_P = 5.5$ $R_{WP} = 7.4$ $R_F(MnAsO_4) = 2.7$ $R_F(Mn_2As_2O_7) = 2.9$

Atomic Parameters

atom	sym positions	*x*	*y*	*z*	*B* (Å^2)[b]
Mn(a)	2a	0.000	0.000	0.000	0.84(7)
Mn(b)	2d	0.500	0.000	0.000	0.45(7)
As	4e	0.2801(2)	0.1805(1)	0.4633(3)	0.76(3)
O(1)	4e	0.2811(10)	0.1162(8)	0.8009(13)	1.0(2)
O(2)	4e	0.7682(12)	0.1274(7)	0.9207(15)	0.8(2)
O(3a)	4e	0.0723(9)	0.1220(8)	0.3155(12)	0.1(2)
O(3b)	4e	0.4764(10)	0.1248(8)	0.3130(14)	0.1(2)

[a] *R*-factors are defined in refs 32 and 33. [b] Isotropic temperature factor.

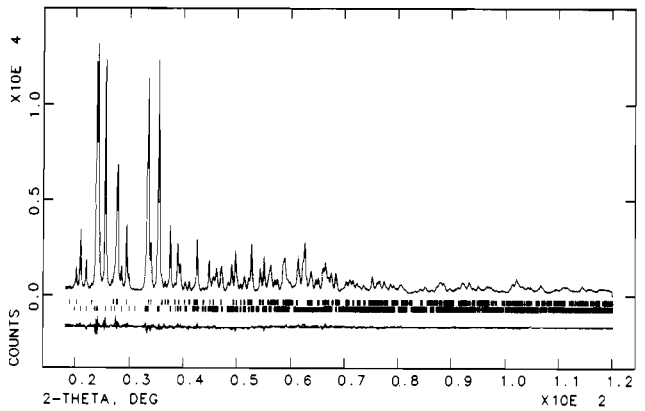

Figure 4. Final observed (points), calculated (full line), and difference X-ray profiles for the mixture of $Mn_2As_2O_7$ and $MnAsO_4$. Reflections bars are shown for $Mn_2As_2O_7$ (top) and $MnAsO_4$ (bottom).

the two phases is found to be 78(1)% $MnAsO_4$ and 22(1)% $MnAsO_{3.5}$ (=$^1/_2$ $Mn_2As_2O_7$).

The structure of the new compound $MnAsO_4$ is the first example of a monoclinically distorted $CuSO_4$ arrangement. Infinite chains of trans-edge-sharing MnO_6 octahedra run parallel to [100] and are linked by highly distorted AsO_4 tetrahedra to give a three-dimensional framework (Figure 5a). The geometry of the infinite chains of octahedra, shown schematically in Figure 6, varies significantly between $CuSO_4$ and $MnAsO_4$. All of the CuO_6 octahedra in the former structure are equivalent and display a typical [4 + 2] Jahn–Teller distortion with two short and two long bridging Cu–O bonds. Each bridging oxygen has either two short or two long bonds to Cu^{2+} (Figure 6a). This results in antiferromagnetic superexchange between neighboring spins in $CuSO_4$[41] and isomorphous $CuSeO_4$[42] as the dσ orbitals containing unpaired electrons are directed toward the same bridging atom. The chains in $MnAsO_4$ have a more complex geometry (see Table III and Figure 6b) as there are inequivalent alternating Mn(a) and Mn(b) sites. Mn(a) shows the [4 + 2] distortion mode, but the Mn(b) environment is better described as an orthorhombic [2 + 2 + 2] distortion. The cooperative Jahn–Teller distortions of the octahedra result in one long and one short bond to each bridging oxygen, which would be expected to result in a ferromagnetic spin–spin coupling within the chains, as the magnetic dσ orbitals on adjacent Mn^{3+} ions cannot overlap with the same bridging atoms. A low-temperature powder neutron diffraction study is planned to determine the magnetic structure of $MnAsO_4$.

The polyhedral representations[43] of the $MnAsO_4$ and $MnAsO_4 \cdot H_2O$ frameworks in Figure 5 illustrate the close relationship

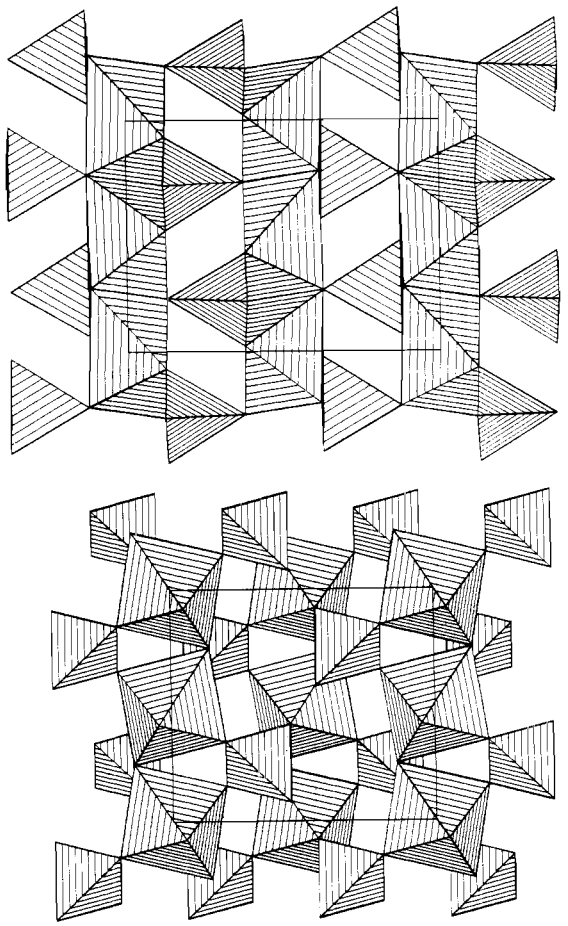

Figure 5. (001) projections of the crystal structures of (a, top) $MnAsO_4$ and (b, bottom) $MnAsO_4 \cdot H_2O$ in the space group $P2_1/n$ (*a*-axis vertical).

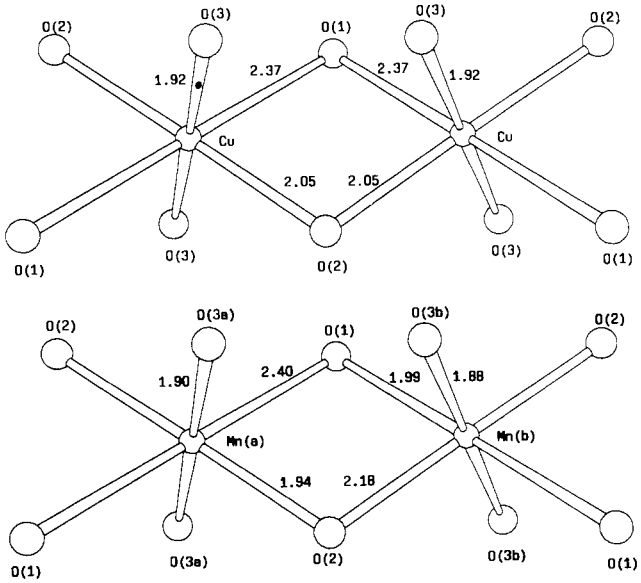

Figure 6. Schematic views of the edge-sharing MO_6 chains in (a, top) $CuSO_4$ and (b, bottom) $MnAsO_4$ with bond distances labeled.

(41) Almodovar, I.; Frazer, B. C.; Hurst, J. J.; Cox, D. E.; Brown, P. J. *Phys. Rev.* **1965**, *129*, A153.
(42) Scharenberg, W.; Will, G. *J. Phys. C1* **1971**, *32*, 851.

Table III. Bond Distances (Å) and Angles (deg) for $MnAsO_4$

Mn(a)–O(1) × 2	2.399(6)	Mn(b)–O(1) × 2	1.985(7)	As–O(1)	1.716(5)
Mn(a)–O(2) × 2	1.940(8)	Mn(b)–O(2) × 2	2.178(7)	As–O(2)	1.729(4)
Mn(a)–O(3a) × 2	1.900(7)	Mn(b)–O(3b) × 2	1.883(7)	As–O(3a)	1.604(5)
				As–O(3b)	1.617(5)
⟨Mn(a)–O⟩	2.08	⟨Mn(b)–O⟩	2.02	⟨As–O⟩	1.67
O(1)–Mn(a)–O(1)	180	O(1)–Mn(b)–O(1)	180	O(1)–As–O(2)	116.2(4)
O(1)–Mn(a)–O(2)	107.7(3)	O(1)–Mn(b)–O(2)	103.4(3)	O(1)–As–O(3a)	104.9(3)
O(1)–Mn(a)–O(3a)	84.5(2)	O(1)–Mn(b)–O(3b)	88.6(3)	O(1)–As–O(3b)	111.4(3)
O(2)–Mn(a)–O(2)	180	O(2)–Mn(b)–O(2)	180	O(2)–As–O(3a)	103.8(3)
O(2)–Mn(a)–O(3a)	92.0(2)	O(2)–Mn(b)–O(3b)	93.2(3)	O(2)–As–O(3b)	106.5(4)
O(3a)–Mn(a)–O(3a)	180	O(3b)–Mn(b)–O(3b)	180	O(3a)–As–O(3b)	114.1(3)
Mn(a)–O(1)–Mn(b)	98.9(3)	Mn(a)–O(1)–As	124.4(4)	Mn(b)–O(1)–As	125.8(4)
Mn(a)–O(2)–Mn(b)	108.4(3)	Mn(a)–O(2)–As	122.0(4)	Mn(b)–O(2)–As	122.0(4)
		Mn(a)–O(3a)–As	134.8(4)	Mn(b)–O(3b)–As	130.5(4)

between the two structures. Loss of the water that links the octahedra into apically-linked chains in $MnAsO_4 \cdot H_2O$ is accompanied by a rotation of the AsO_4 tetrahedra to give edge-sharing chains in $MnAsO_4$. The Mn···Mn distance within the chains of octahedra decreases from 4.05 Å in $MnAsO_4 \cdot H_2O$ to 3.34 Å in $MnAsO_4$. The observed reversibility of this transformation reflects the fact that only some weak Mn–O bonds are broken, accompanied by rotations of the arsenate groups.

Conclusions

Electron microscopy, density, thermal, and analytical powder diffraction measurements suggest that $MnXO_4 \cdot nH_2O$ (X = P, As) compositions with $n > 1$ are intergrowths of crystalline $MnXO_4 \cdot H_2O$ and an amorphous precursor phase of average composition $MnXO_4 \cdot 4H_2O$, although a mixture of these phases with variable particle size cannot be discarded. The detailed thermal analyses of these materials show that the arsenate alone can be dehydrated without losing oxygen, leading to the synthesis of the simple new solid $MnAsO_4$. This compound adopts a novel monoclinically-distorted $CuSO_4$-type structure in which chains of edge-sharing MnO_6 octahedra displaying cooperative [4 + 2] and [2 + 2 + 2] Jahn–Teller distortions are linked through distorted AsO_4 groups. These chains are predicted to show ferromagnetic spin–spin coupling.

Acknowledgment. We thank the British Council and Ministerio de Educacion y Ciencia (Spain) for funding from the Acciones Integradas Programme. We also thank Miss Nicola Steadman for her help with the electron microscopy which was performed at the Chemical Crystallography Laboratory, University of Oxford. The work in Málaga was supported by CICYT Research Grant MAT-90-298. M.A.G.A. thanks the Spanish Government for a Studentship and the EC for a Human Capital and Mobility Research Fellowship.

(43) Fischer, R. X. *J. Appl. Crystallogr.* **1985**, *18*, 258.